On the transport of heavy particles through a downward displacement-ventilated space

Nicola Mingotti[12]†, Andrew W. Woods[1]

[1]BP Institute, University of Cambridge, Madingley Road, Cambridge CB3 0EZ, UK
[2]Department of Architecture, University of Cambridge, Cambridge CB2 1PX, UK

(Received ?; revised ?; accepted ?. - To be entered by editorial office)

We investigate the transport of relatively heavy, small particles through a downward displacement-ventilated space. A flux of particles is supplied to the space from a localised source at a high level and forms a turbulent particle-laden plume which descends through the space. A constant flow of ambient fluid which does not contain particles is supplied to the space at a high level, while an equal amount of fluid is vented from the space at a low level. As a result of the entrainment of ambient fluid into the particle plume, a return flow is produced in the ambient fluid surrounding the plume in the lower part of the space. At steady state, particles are suspended by this return flow. An interface is formed which separates the ambient fluid in the lower part of the space, which contains particles, from the particle-free ambient fluid in the upper part of the space. New laboratory experiments show that the concentration of particles in the ambient fluid below the interface is larger than the average concentration of particles in the plume fluid at the level of the interface. Hence, as the plume fluid crosses the interface and descends through the particle-laden fluid underneath, it becomes relatively buoyant and forms a momentum-driven fountain. If the fountain fluid impinges on the floor, it then spreads radially over the surface until lifting off. We develop a quantitative model which can predict the height of the interface, the concentration of particles in the lower layer, and the partitioning of the particle flux between the fraction which sediments over the floor and that which is ventilated out of the space. We generalise the model to show that when particles and negatively-buoyant fluid are supplied at the top of the space, a three-layer stratification develops in the space at steady state: the upper layer contains relatively low-density ambient fluid in which no particles are suspended; the central layer contains a mixture of ambient and plume fluid in which no particles are suspended; and the lower layer contains a suspension of particles in the same mixture of ambient and plume fluid. We quantify the heights of the two interfaces which separate the three layers in the space and the concentration of particles in suspension in the ambient fluid in the lower layer. We then discuss the relevance of the results for the control of airborne infections in buildings. Our experiments show that the three-layer stratification is subject to intermittent large-scale instabilities when the concentration of particles in the plume at the source is sufficiently small, or the rate of ventilation of the space is sufficiently large: we describe the transient concentration of particles in the space during one of these instabilities.

Key words: Particles, contaminants, stratification, ventilation

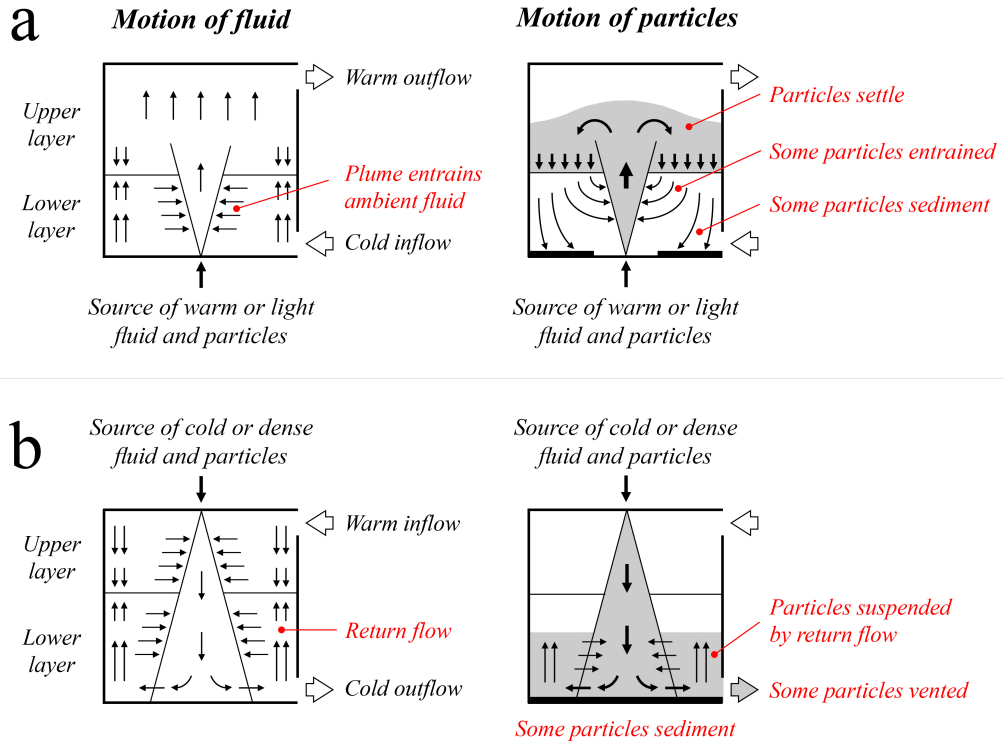

FIGURE 1. Schematics illustrating the motion of fluid and relatively heavy small particles through an upward and a downward displacement-ventilated space (a and b respectively.)

1. Introduction

The study of how a suspension of particles is transported through an enclosed space is relevant to a variety of environmental and engineering problems, including the transport of crystals through a magma chamber (Martin & Nokes 1989) and the transport of colloids through multi-phase fluid (Frank & Prost 2009). In chemical reaction vessels, catalyst particles and a flux of feedstock fluid may be added at high level to the vessel (cf. Nienow *et al.* 1997, Werther 2007). In this case, a descending plume containing fluid and catalyst particles is formed in the vessel, and the catalyst particles are transported by the plume to the base of the vessel.

In buildings, suspensions of relatively heavy particulate contaminants are frequently generated (Atkinson *et al.* 2009). To preserve a healthy indoor environment, contaminants can be removed by ventilation. In low-energy buildings, thermal stratification is frequently used to drive the ventilation flows through a room which contains a source of heating or cooling (Linden *et al.* 1990; Gladstone & Woods 2001). In a thermally-stratified space, the level at which ventilation is supplied to the space is different to the level at which exhaust air is vented from the space (see figure 1). In cold seasons or climates, an upward air flow is produced through a ventilated space which contains a source of heating (figure 1a), while in warm seasons or climates air flows downwards through a space which contains a source of cooling (figure 1b). The interaction between a suspension of relatively heavy particles and the background ventilation flow changes when the ventilation direction is changed. In figure 1a, particles settle downwards through a

† Email address for correspondence: nm441@cam.ac.uk

background upward ventilation flow, while in figure 1b particles fall in the same direction as the descending ventilation flow. This leads to different particle dispersal patterns through the space.

In a companion paper, Mingotti & Woods (2015) recently investigated the transport of small, heavy particles which are released in a localised source of buoyant fluid at the base of a space with an upward background flow (figure 1a). Laboratory experiments demonstrated that if the flux of particles which are supplied to the space is small, a buoyant particle-laden plume develops, which rises through the space while entraining ambient fluid. At steady-state, a two-layer density stratification is formed in the space (see figure 1a). In the upper part of the space, particles mix with the ambient fluid and settle. Unless the rate of ventilation of the space is very large, only a fraction of the supplied particles are transported to the top of the space and vented to the exterior through the high-level opening, while the remaining particles sediment within the space and eventually deposit onto the floor. While settling through the ambient fluid, some particles are entrained by the plume in the lower layer and re-suspended into the upper layer (figure 1a): such recirculation increases the concentration of particles in suspension in the ambient fluid, changing the balance between the sedimentation and the ventilation of the particles.

In the present paper, motivated by the processes of particle transport in confined spaces or vessels in which there is a net background flow, we examine the fluid flows which develop when a flux of small, heavy particles are released in a localised source of negatively-buoyant fluid at the top of a space with downward displacement ventilation (figure 1b). In this case, a descending turbulent plume is formed, and all the particles which are released at the plume source are transported from the top of the space to its base. As a result of entrainment of ambient fluid by the plume, a return flow develops in the ambient (Linden *et al.* 1990). In the lower part of the space, the upward speed of this flow may exceed the speed at which particles settle through the ambient fluid. If this happens, particles become suspended and a layer of particle-laden fluid is formed (figure 1b). Particles in this layer can either be vented from the space through the low-level outlet vent, or sediment onto the floor of the space.

The aim of this paper is to investigate the effectiveness of the downward background flow at removing particles from such an enclosed space. Based on the results of a series of new laboratory experiments, we develop a theoretical model which quantifies the fraction of particles which are extracted from the space at low level, and the fraction of particles which sediment within the space at steady state. We also quantify the depth of the layer of particle-laden fluid at the base of the space and the concentration of particles in this layer at steady state for different particle fluxes and rates of ventilation of the space.

The structure of the paper is as follows. In section 2, we consider the simpler case in which particles and neutrally-buoyant fluid are supplied from a localised source into an enclosed space with a net downward background flow. We present a series of new experiments and develop a model to quantify the concentration of particles in the ambient fluid in the lower part of the enclosure (see figure 1b). Experimental results indicate that this concentration is larger than the concentration of particles in the plume fluid. Consequently, the plume fluid becomes relatively buoyant compared with the surrounding ambient fluid, and a momentum-driven fountain is formed in the lower part of the space. In section 3 we describe this fountain and explore how the sedimentation of particles onto the floor of the enclosure is affected by the fountain flow. In section 4, we consider the more general case in which particles and negatively-buoyant fluid are supplied from a localised source into the space. Our experiments indicate that the distribution of particles in the space can be subject to intermittent large-scale instabilities when particles

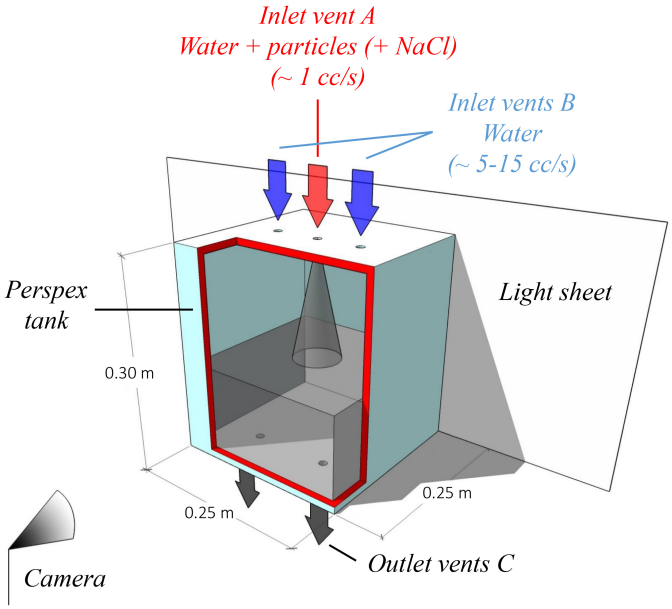

FIGURE 2. Schematic illustrating the laboratory setup.

and negatively-buoyant fluid are supplied to the space: we describe these instabilities in section 5. In section 6 we consider the implications of our model for infection control in buildings.

2. Plume containing particles and neutrally-buoyant fluid

2.1. *Experiments*

Figure 2 illustrates the experimental setup. A perspex tank of internal dimensions 25 x 25 x 30 cm is filled with water. The tank incorporates a series of low- and high-level openings, through which clear and particle-laden fluid are pumped. Fresh water containing particles is supplied to the tank through an opening located at the centre of the tank's top surface (vent A in figure 2). This particle-laden fluid passes through a glass nozzle of an internal diameter 4.2 mm: the vertical distance between the tip of the nozzle and the tank's floor is 26 cm. Two holes of diameter 8.2 mm are drilled at high level in the tank (vents B in figure 2) and are used as inlets for the background flow. Through these holes, fresh water is supplied to the tank at a constant rate during the experiment. The base of the tank incorporates two outlet openings of diameter 8.2 mm (vents C in figure 2). Through these vents, fluid is extracted from the tank over the course of an experiment.

In all experiments, the particle-laden fluid is supplied to the tank at a constant volume flux of 1 cm^3/s using a peristaltic pump (Watson Marlow). This kind of pump generates a pulsed input condition. In our experiments, the pump frequency is of order 10 Hz, and so the time lapse between two pulses produced by the pump (a fraction of a second) is very small compared with the time required for a change in the distribution of particles in the tank (several seconds or minutes). Hence, the input condition is approximated as a continuous flow of particle-laden fluid supplied to the tank. To explore the impacts of larger or smaller particle fluxes, the concentration of particles in this fluid, C_{in}, is changed throughout the series of experiments (cf. table 1). The ventilation fluid is also

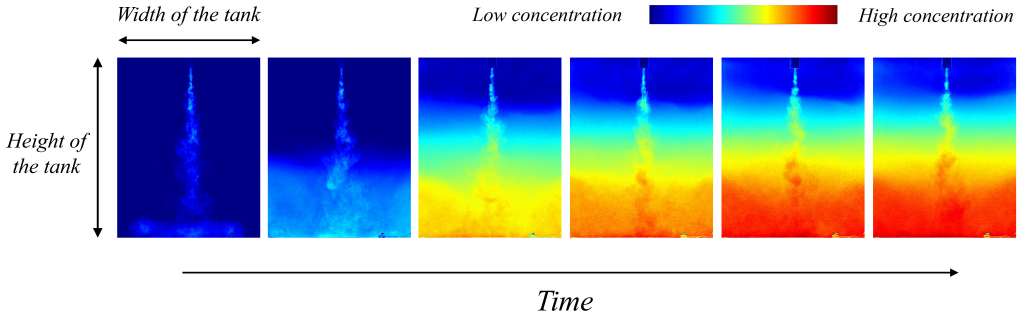

FIGURE 3. Transient concentration of particles in suspension in the tank during experiment b (cf. table 1). A series of images illustrate the concentration distribution in the tank at the following times after the beginning of the experiment: 30 seconds and 5, 28, 43, 70 and 86 minutes.

Experiment	$Q \cdot 10^{-6}$	$C_{in} \cdot 10^{-3}$	$B_p \cdot 10^{-8}$
a	10	5.35	11.6
b	5	5.35	11.6
c	10	3.57	7.8
d	10	2.30	5.0
e	10	1.78	3.9
f	5	0.76	1.7
g	15	5.35	11.6

TABLE 1. List of the laboratory experiments described in section 2. In this set of experiments, the floor area of the tank and the mean settling speed of the particles are fixed at $A = 6.25 \cdot 10^{-2}$ m^2 and $\bar{v}_s = 0.40 \cdot 10^{-3}$ m/s respectively. Q (m^3/s) denotes the rate at which the ambient fluid is vented from the tank through the low-level opening; C_{in} (m^3 particles / m^3 water) is the concentration of particles in the plume fluid at the source; and B_p (m^4/s^3) the buoyancy flux associated with particles in the plume fluid.

pumped into the tank at different flow rates, ranging between 5 and 15 cm^3/s, to explore the impacts of a larger or smaller ventilation of the space (cf. table 1).

Silicon carbide particles of mean diameter 18.3 μm and of mean settling speed $\bar{v}_s = 4.04 \cdot 10^{-4}$ m/s are used in the experiments (Carborex F400 by Washington Mills). The distribution of settling speeds about the mean was measured using a combination of a settling experiment and of an optical particle characterisation experiment (Mingotti & Woods 2015). A graph showing the distribution of settling speeds in the mixture of particles used in the experiments is given in appendix A (figure 19).

We use an image-analysis technique to assess the average line-of-sight concentration of particles in suspension in the fluid. An electroluminescent light sheet is connected to the rear of the tank and provides uniform illumination (see figure 2). The light produced by this sheet is attenuated if the fluid contains a suspension of particles. During an experiment, we take photographs of the tank using a Nikon D90 digital camera and based on the light intensity relative to a set of calibration values, we infer the line-of-sight average concentration of particles in the tank (cf. appendix B and Mingotti & Woods 2015).

An experiment is started when a flow of particle-laden fluid is supplied to the tank through vent A. The bulk density of this fluid is larger than that of the ambient fluid, which does not contain particles. As a result, the particle-laden fluid forms a turbulent plume, which descends through the tank while entraining ambient fluid. On reaching the

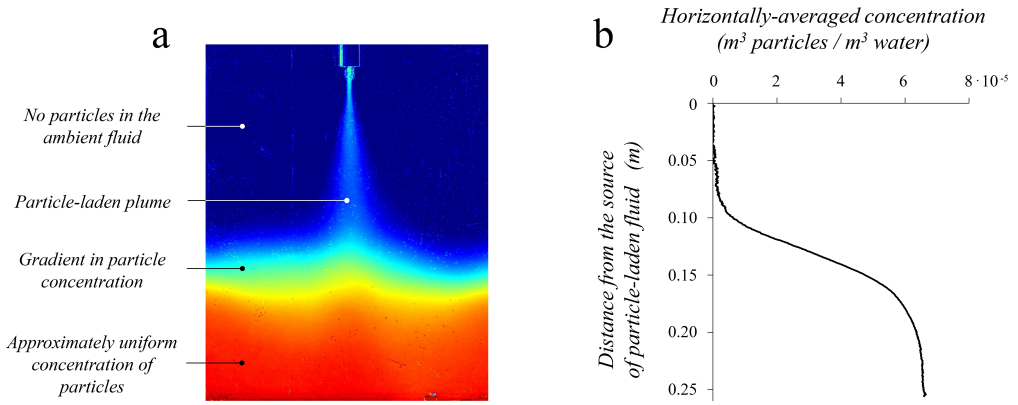

FIGURE 4. Steady-state distribution of particles in the tank in a typical experiment (experiment e, cf. table 1). Image a) illustrates the steady-state concentration of particles in the tank using false colours; image b) shows the horizontally-averaged particle concentration profile.

base of the tank, the particle-laden fluid spreads radially over the floor (see figure 3, first image on the left-hand side). A certain number of particles become suspended in the ambient fluid in the lower part of the tank (see figure 3, second and third images from the left). Over the course of the experiment, the concentration of particles in the ambient fluid increases and so observing the motion of the plume fluid in the lower part of the tank becomes increasingly difficult. Eventually, a steady state is reached (see figure 3, images on the right-hand side).

Figure 4 shows the average of 1000 frames of experiment e (cf. table 1) once it has reached steady state, corresponding to 500s of experimental time. Figure 4a is a false-colour image which illustrates the difference in the average concentration of particles through the tank. Figure 4b shows the horizontal average of the concentration at each level in the tank. Figures 4a and b show that at steady state particles are not uniformly distributed in the tank. In the upper part of the tank the ambient fluid does not contain particles at steady state (dark blue colour in the false-colour image). The particle-laden plume originates at the top of the tank, and descends through the enclosure while entraining ambient fluid (light blue colour in figure 4a). In the central part of the tank, at an approximate distance 0.10-0.15 m below the source of particle-laden fluid, we observe a vertical gradient in the concentration of particles in the ambient fluid (note the light blue/yellow colours in figure 4a, and the change in the horizontally-averaged particle concentration profile plotted in figure 4b). In the lower part of the tank, the ambient fluid contains a relatively large number of particles (red colour in the false-colour image). The concentration of these particles is approximately uniform (see figure 4b, in which the particle concentration becomes approximately uniform at a distance 0.20-0.22 m below the source of the particle-laden fluid).

Motivated by the outcomes of the experiments, we develop a model based on plume theory which describes the transport of small, heavy particles through a space with downward ventilation. In section 2.2, we describe the particle-laden turbulent plume which is originated at the top of the space when particles are supplied from a localised source located at high level (see figures 3 and 4). The plume descends through the space while entraining ambient fluid, and so a return flow is produced in the ambient fluid in the lower part of the space (see figure 1b). In section 2.3, we describe how particles of different sizes are suspended in the ambient fluid by this return flow. In section 2.4, we

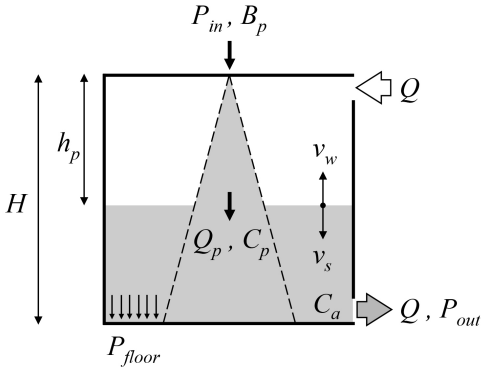

FIGURE 5. Schematic showing the conditions used in the modelling (section 2).

quantify the steady-state concentration of particles in the ambient fluid at the base of the space, and we compare the predictions of our model with the results of the experiments.

2.2. *Particle-laden plume*

We assume that the space is of a height H and of a cross-sectional area A, and is ventilated at a steady rate Q (figure 5). The ventilation flow is supplied to the space at high level and extracted from the space at low level. A constant flux of relatively heavy small particles are supplied to the space at high level. We denote this flux by P_{in}. A turbulent particle-laden plume is originated at the top of the enclosure, and the plume fluid descends through the space driven by negative buoyancy flux B_p

$$B_p = P_{in}\frac{\rho_P - \rho_W}{\rho_W}g \tag{2.1}$$

in which ρ_P is the density of the particles, ρ_W is the density of the ambient fluid, and g is gravitational acceleration. While descending through the space, the plume entrains ambient fluid. If the fall speed of the particles is much smaller than the speed of the plume, the particle-laden fluid in the plume behaves analogously to that in a single-phase descending plume (cf. Woods 2010; Zarrebini & Cardoso 2000), and so plume theory indicates that at a vertical distance z from the source, the volume flux is given by

$$Q_p(z) = \lambda B_p^{\frac{1}{3}} z^{\frac{5}{3}} \tag{2.2}$$

in which λ is a universal constant which depends on the plume entrainment coefficient α (Morton *et al.* 1956). When the plume volume flux, Q_p, exceeds the ventilation flux, Q, an upward return flow is produced in the ambient fluid (see figure 1b). So long as the plume's cross-sectional area is much smaller than the tank's floor area, A, we estimate that the ambient fluid rises through the space at a mean speed

$$v_w(z) = \frac{Q_p(z) - Q}{A} \quad , \quad z > \frac{Q^{\frac{3}{5}}}{\lambda^{\frac{3}{5}} B_p^{\frac{1}{5}}} \tag{2.3}$$

Equations 2.1-2.3 are used to measure the properties of the particle-laden plume observed during the experiments (see figures 3 and 4a). Before the beginning of an experiment, some dye is added to a layer of ambient fluid at the base of the tank. We measure the speed at which the dyed fluid rises as a result of the return flow in the lower part of the tank and use equation 2.3 to infer the plume flow rate Q_p at different levels in the tank. We then use equation 2.2 to estimate that in our experiments the particle-laden

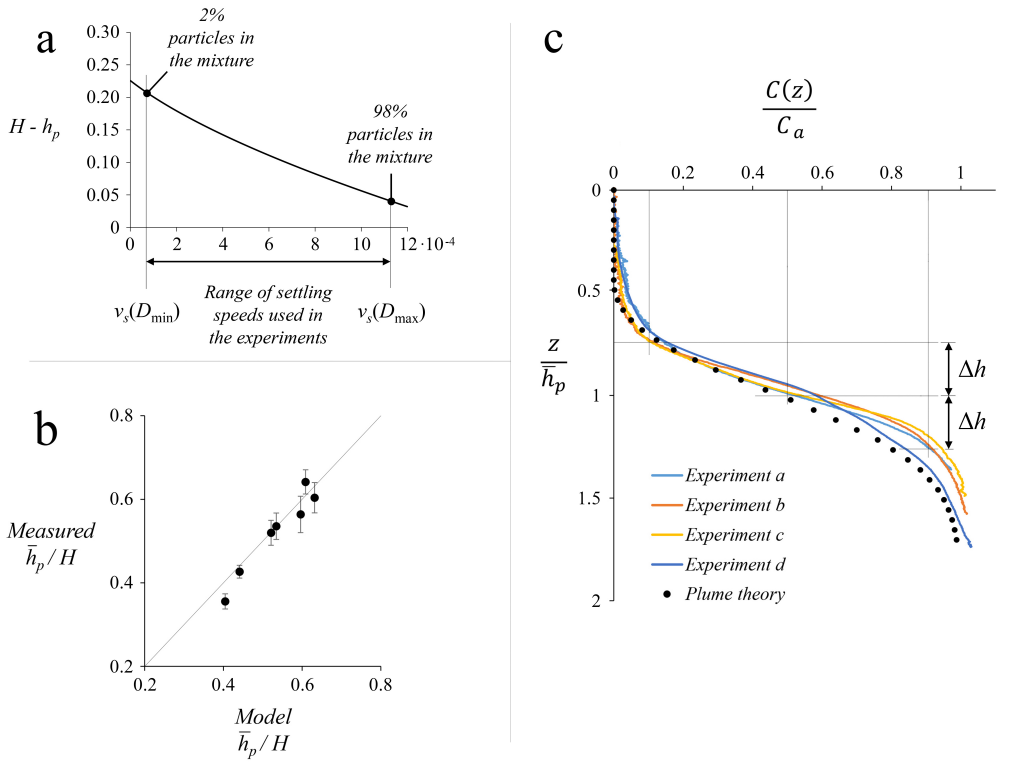

FIGURE 6. a) Range of distances from the floor of the tank, $H - h_p(v_s)$ (m), at which particles with different fall speeds v_s (m/s) are suspended in the ambient fluid in a typical experiment with $Q = 10 \cdot 10^{-6}$ m^3/s and $B_p = 7 \cdot 10^{-8}$ m^4/s^3 (cf. table 1); b) Vertical distance between the source of the plume and the height at which particles with a mean fall speed $\bar{v}_s$ are suspended in the ambient fluid, $\bar{h}_p$. For each one of the experiments listed in table 1, we compare the distance measured in the experiment with the distance predicted by equation 2.5; c) Comparison of the steady-state particle concentration profiles obtained in a number of experiments (lines) with the prediction of the model (dots). In plotting the dotted curve in the figure, we use equation 2.3 to calculate the mean upward speed of the ambient fluid at different levels in the tank, $v_w(z)$. In our experiments, we use particles with a range of settling speeds (cf. appendix A). For a given ambient fluid speed $v_w(z)$, we estimate the fraction of particles in the mixture which have a settling speed $v_s < v_w(z)$ (see figure 19). These particles are sufficiently small that they can be suspended by the return flow. The dotted curve in figure 6c illustrates how this fraction of suspended particles changes at different levels in the tank. We observe that the concentration of the suspended particles increases rapidly in the zone $\bar{h}_p - \Delta h < z < \bar{h}_p + \Delta h$.

plume has a coefficient $\lambda = 0.17 \pm 0.01$, which is consistent with the estimates of Bower *et al.* (2008) and Kuesters & Woods (2011). The same equations are also used to estimate that the virtual origin of the plume is located at a distance $z_0 = 7.9 \pm 2.0$ mm above the tip of the glass nozzle through which the particle-laden fluid is pumped into the tank (vent A in figure 2).

2.3. *Suspension of particles in the ambient fluid*

If the upward speed of the return flow exceeds the speed at which particles settle, particles become suspended in the ambient fluid (cf. Phillips & Woods 2001). Equation 2.3 indicates that the speed at which the ambient fluid rises through the space, v_w, equals

the speed at which a particle settles through the fluid, v_s, when the plume volume flux reaches the critical level

$$Q_{p,crit} = Q + Av_s \tag{2.4}$$

Using a combination of equations 2.2 and 2.4, we calculate that this happens at a vertical distance h_p from the plume virtual origin

$$h_p = \frac{(Q + Av_s)^{\frac{3}{5}}}{\lambda^{\frac{3}{5}} B_p^{\frac{1}{5}}} \tag{2.5}$$

Equation 2.5 indicates that particles with different settling speeds are suspended at different levels in the space by the upward return flow. We use equation 2.5 to calculate the maximum vertical distance from the floor of the tank, $H - h_p(v_s)$, at which particles with different fall speeds are suspended in our experiments. Figure 6a shows that in a typical experiment in which the tank is ventilated at a rate $Q = 10 \cdot 10^{-6}$ m^3/s and a flux of particles with buoyancy $B_p = 7 \cdot 10^{-8}$ m^4/s^3 is supplied at the top of the tank (cf. table 1), all particles used in the experiment can be suspended a distance $H - h_p \leqslant$ 5-20 cm approximately above the base of the tank, with the lower limit corresponding to the larger particles in the mixture and the upper limit corresponding to the smaller particles in the mixture (cf. appendix A). This is consistent with the experimental results illustrated by figures 4a and b, which show that the concentration of particles is approximately uniform in the lower 4-5 cm of the tank, and decreases gradually to zero by a distance of approximately 15-18 cm above the floor.

Since all particles in the mixture are suspended in the ambient fluid at the base of the tank, we can identify the maximum height at which particles with a mean settling speed $\bar{v}_s$ are suspended in the ambient fluid by detecting the level at which the horizontally-averaged mean concentration of particles in the tank is reduced by 50% relative to the maximum concentration at the base of the tank. We denote the vertical distance between the source of the plume and this height by $\bar{h}_p$. For each one of the experiments listed in table 1, we compare the height $\bar{h}_p$ measured during the experiment with that predicted by equation 2.5 for $v_s = \bar{v}_s$ (figure 6b). We observe that there is a relatively good agreement between model predictions and experimental results, with errors of less than 5% in most experiments.

In figure 6c, we compare the horizontally-averaged mean particle concentration profiles obtained in a number of experiments (coloured lines) with the profile predicted by the model (black dots, plotted using equation 2.5). The profiles are plotted in dimensionless form: particle concentration is scaled by the maximum concentration at the base of the tank, C_a, while height is scaled by $\bar{h}_p$ (see figure 6b). The graph shows that the model based on plume theory provides a leading order prediction of the horizontally-averaged mean concentration of particles at different levels in the tank, with average errors of order 5-10% approximately. However, we observe that the magnitude of errors increases to 15-20% at the base of the tank. In section 3 we will demonstrate that the particle-laden plume transitions into a momentum-driven fountain in the lower part of the tank. As a result of the difference between the descending volume fluxes in the plume and in the fountain, the effective speed of the return flow in the lower part of the tank will be different than that predicted by equation 2.3. This explains why the model prediction based on plume theory (black dots in figure 6c) is less accurate in this region.

In figure 6c we also observe that the distribution of settling speeds in the mixture of particles used in the experiments is sufficiently narrow that the fraction of particles suspended in the ambient fluid rapidly increases from 10% to 90% in a relatively small region in the tank, $\bar{h}_p - \Delta h < z < \bar{h}_p + \Delta h$, with $\Delta h \approx$ 3-4 cm (cf. appendix A).

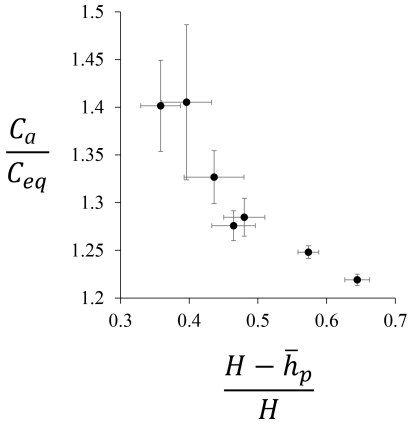

FIGURE 7. The measured concentration of particles at the base of the tank, C_a, is compared with the concentration C_{eq} given by equation 2.16. We observe that in our experiments C_a is consistently larger than C_{eq}.

2.4. *Concentration of particles in the ambient fluid at the base of the space*

After quantifying the maximum height at which particles are suspended in the ambient fluid, we now develop a model based on plume theory to quantify the concentration of particles in the suspension. For convenience, we first consider the simpler case in which all particles have uniform diameter D and settling speed v_s. We then consider the more general case in which particles with different diameters and settling speeds are supplied to the space.

Equation 2.5 indicates that if all particles have a uniform fall speed v_s, an interface is formed at a distance h_p from the plume source (cf. equation 2.5): the interface separates the ambient fluid in the upper part of the space, which does not contain particles, from the ambient fluid in the lower part of the space, which contains a suspension of particles (figure 5). The concentration of particles in the plume fluid at the level of the interface is given by

$$C_p\left(h_p\right) = \frac{P_{in}}{Q_{p,crit}} = \frac{P_{in}}{Q + Av_s} \tag{2.6}$$

To calculate the concentration of particles in the ambient fluid below the interface, we note that at steady state the flux of particles supplied to space, P_{in}, is balanced by the combination of the flux of particles vented from the space, P_{out}, and the flux of particles which sediment over the floor, P_{floor} (figure 5)

$$P_{in} = P_{floor} + P_{out} \tag{2.7}$$

Motivated by the experimental results (e.g. figure 4a) we assume that particles are well-mixed horizontally near the base of the space, and we denote the uniform concentration of particles at the level of the floor by C. The flux of particles vented from the space is then given by

$$P_{out} = QC \tag{2.8}$$

If particles sediment uniformly over the entire floor area at a speed v_s, the flux of particles which deposit onto the floor at steady state is given by

$$P_{floor} = Av_sC \tag{2.9}$$

A combination of equations 2.7-2.9 indicate that if particles are well-mixed in the ambient fluid below the interface and sediment uniformly over the entire floor area, the concentration of particles at the base of the space reaches the equilibrium value at steady state

$$C_{eq} = \frac{P_{in}}{Q + Av_s} \tag{2.10}$$

In this case, the concentration of particles in the ambient fluid below the interface equals the concentration of particles in the plume fluid at the level of the interface (cf. equations 2.6 and 2.10).

We now extend the model to consider the more general case in which particles of different sizes and settling speeds are supplied to the space. We assume that all particles in the mixture are suspended in the ambient fluid at the base of the space (see figure 6a). In this case the flux of particles vented from the tank, P_{out}, and the flux of particles which sediment onto the floor, P_{floor}, are given by

$$P_{out} = Q \int_{D_{min}}^{D_{max}} c_b\left(D\right) dD \tag{2.11}$$

and

$$P_{floor} = A \int_{D_{min}}^{D_{max}} v_s\left(D\right) c_b\left(D\right) dD \tag{2.12}$$

respectively. In equations 2.11 and 2.12, D denotes particle diameter, which ranges between D_{min} and D_{max} (see figure 6a), and $c_b\left(D\right)$ represents the particle concentration density function just above the base of the tank, so that the total concentration of all the particles suspended just above the base of the tank is

$$C = \int_{D_{min}}^{D_{max}} c_b\left(D\right) dD \tag{2.13}$$

For each particle size D, conservation of particles requires that (cf. equation 2.7)

$$p_{in}\left(D\right) = Qc_b\left(D\right) + Av_s\left(D\right) c_b\left(D\right) \tag{2.14}$$

where $p_{in}\left(D\right)$ is the density function of the concentration flux supplied to the space such that

$$P_{in} = \int_{D_{min}}^{D_{max}} p_{in}\left(D\right) dD \tag{2.15}$$

Using equations 2.11-2.15, we calculate the mean concentration of particles at the base of the tank, C_{eq}, at which the flux of particles supplied to the space is balanced by the combination of the flux of particles vented from the space and the flux of particles which sediment over the entire floor area (cf. equation 2.10)

$$C_{eq} = \int_{D_{min}}^{D_{max}} \frac{p_{in}\left(D\right)}{Q + Av_s\left(D\right)} dD \tag{2.16}$$

For each one of the experiments listed in table 1, we compare this concentration with the mean concentration of particles which we measured during the experiment at a vertical distance 2 cm from the base of the tank, C_a. Figure 7 shows that in all our experiments the measured concentration at the base of the tank exceeds the concentration predicted by equation 2.16 by 20-40%. We observe that the difference between C_a and C_{eq} increases when the vertical distance between the floor of the tank and the height at which particles

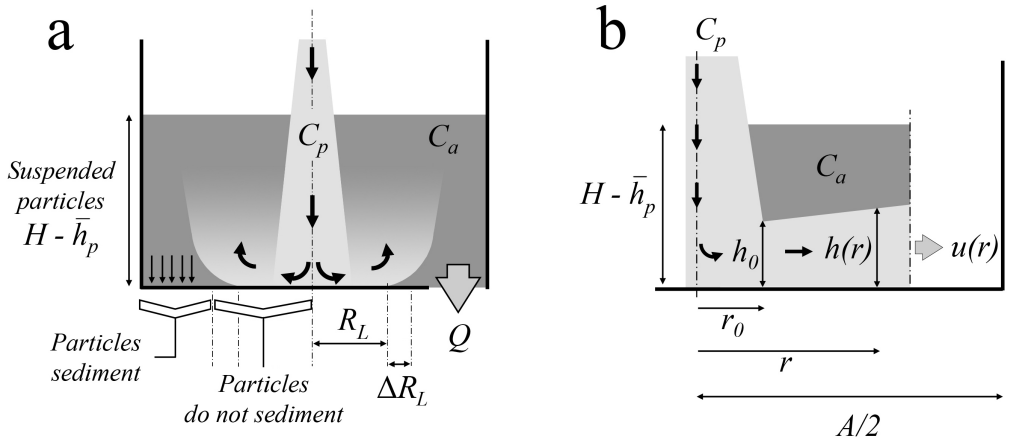

FIGURE 8. Particle-laden fountain impinging on the floor (section 3).

with a mean settling speed $\bar{v}_s$ are suspended, $H - \bar{h}_p$, is reduced. We now develop the model to account for this difference by modelling the interaction of the plume fluid with the floor of the tank.

3. Particle-laden fountain

Figure 7 shows that in our experiments the concentration of particles in the ambient fluid in the lower part of the tank is always significantly larger than the concentration given by equation 2.16, and so the bulk density of the ambient fluid is larger than that of the plume fluid in the lower layer (cf. equations 2.6 and 2.10). We therefore expect the plume to transition into a momentum-driven fountain which descends through the relatively dense ambient fluid in the lower part of the tank. In this section, we explore the flow of the fountain fluid and investigate the conditions at which the fountain fluid reaches the base of the space and impinges on the floor (figure 8a). We then explore how the fountain fluid propagates at the level of the floor: we show that the fluid spreads over the floor radially, until it reaches a critical radius R_L at which it separates from the floor surface and lifts off due to its reduced density relative to the density of the surrounding ambient fluid (figure 8a). Finally, we investigate how the vigorous motion of the fountain fluid at the level of the floor may reduce the effective area over which particles sediment onto the floor.

As a result of the distribution of settling speeds in the mixture of particles supplied to the tank, in our experiments we observe a continuous stratification in particle concentration (see figures 4 and 6) rather than a sharp interface between the upper and the lower layer (as depicted diagrammatically in figure 5). Consequently, the bulk density of the ambient fluid increases gradually in the lower part of the tank, and so it is difficult to determine the exact height at which the plume fluid becomes less dense than the surrounding ambient fluid in each experiment. However, in section 2.3 we noted that the distribution of settling speeds in the mixture of particles used for the experiments is narrow, and so the concentration of particles in the ambient fluid increases rapidly in the region $\bar{h}_p - \Delta h < z < \bar{h}_p + \Delta h$ (see figure 6c). Consequently, in developing our model, we will assume as a simplification that the plume transitions into a fountain at a distance $H - \bar{h}_p$ above the floor of the tank, where particles with the mean fall speed $\bar{v}_s$ are suspended by the return flow in the ambient fluid as described in section 2.2. For the

same reason, we will also assume for simplicity that the mean concentration of particles in the plume fluid at a distance $\bar{h}_p$ from the source is given by equation 2.6.

3.1. *Particle-laden fountain in the lower part of the space*

We assume that at a distance $z = \bar{h}_p$ below the source the plume fluid enters a layer of ambient fluid with a mean concentration of particles $C_a > C_p\left(\bar{h}_p\right)$. On entering this layer of relatively dense ambient fluid, the plume fluid has an upward buoyancy flux B_f relative to the surrounding ambient fluid

$$B_f = \left(C_a - C_p\left(\bar{h}_p\right)\right)\frac{\rho_P - \rho_W}{\rho_W} g\left(Q + A\bar{v}_s\right) = \hat{C}B_p \tag{3.1}$$

in which

$$\hat{C} = \frac{C_a - C_p\left(\bar{h}_p\right)}{C_p\left(\bar{h}_p\right)} \tag{3.2}$$

is the fractional difference between the mean concentration of particles in the ambient fluid and that in the plume fluid. Equation 2.4 indicates that at this level the plume fluid has a momentum flux M_f

$$M_f = \frac{\left(Q + A\bar{v}_s\right)^2}{\pi r_p^2} \tag{3.3}$$

in which

$$r_p = \frac{6}{5}\alpha\bar{h}_p \tag{3.4}$$

is the radius of the plume at a distance $\bar{h}_p$ below the source (Morton *et al.* 1956). As a result of the upward buoyancy flux B_f combined with the momentum flux M_f, the plume transitions into a momentum-driven fountain. Literature on turbulent fountains, including Turner (1966), Mizushina *et al.* (1982), Bloomfield & Kerr (1998, 2000) and Burridge & Hunt (2012), indicates that in a deep layer of fluid the maximum distance travelled by such a fountain, h_f, is given by

$$h_f = \gamma M_f^{\frac{3}{4}} B_f^{-\frac{1}{2}} \tag{3.5}$$

in which γ is a constant of order 1. In a set of experiments on turbulent fountains, Bloomfield & Kerr (2000) measured $\gamma = 1.70 \pm 0.17$; similar results were obtained by the other researchers cited above.

In our experiments, with $\hat{C} \approx$ 0.2-0.4 (see figure 7), the upward buoyancy flux of the fountain fluid relative to the surrounding particle-laden ambient fluid is of order $B_f \approx 10^{-8}$ m^4/s^3 (cf. equation 3.1 and table 1). For a typical plume radius at the level of the interface $r_p \approx$ 2-3 cm and a typical rate of ventilation of the tank $Q \approx 10 \cdot 10^{-6}$ m^3/s, the momentum flux of the fountain fluid at the interface is of order $M_f \approx 10^{-6}$ m^4/s^2 (cf. equation 3.3). Consequently, equation 3.5 indicates that $h_f \approx$ 0.3-0.5 m. This length exceeds the typical depth of the layer in which particles with a mean settling speed $\bar{v}_s$ are suspended in the ambient fluid in the tank, $H - \bar{h}_p \approx$ 0.1-0.2 m. Hence, the fountain fluid reaches the bottom of the tank and impinges on the floor in our experiments (figure 8a).

3.2. *Motion of the fountain fluid at the level of the floor*

When the fountain fluid reaches the bottom of the tank, it initially spreads radially over the floor, but then lifts off from the floor surface at a radial distance R_L from the fountain vertical axis as a result of its buoyancy relative to the particle-laden ambient

fluid (figure 8a). Cooper & Hunt (2004, 2007) ran a series of experiments to explore the behaviour of a turbulent fountain containing fresh water in a relatively dense environment containing a solution of water and salt. They observed that when the fountain impinges perpendicularly on a floor, the critical radius R_L is given by

$$R_L = \varepsilon \pi^{-\frac{3}{8}} \gamma^{-\frac{3}{2}} \frac{h_f^{\frac{3}{2}}}{\left(H - \bar{h}_p\right)^{\frac{1}{2}}} \tag{3.6}$$

in which $\varepsilon = 0.03$ is a coefficient which Cooper & Hunt (2007) obtained by an empirical fit of their experimental results. In our experiments, the fountain fluid contains particles, which are subject to gravitational settling and may fall out of the fountain fluid as it spreads over the floor. Equation 3.6 can be used to estimate the critical radius at which the particle-laden fountain fluid lifts off from the floor surface only if the fraction of particles which fall out of the fluid as it spreads over the floor is small. If this is the case, then in our experiments we estimate $R_L \approx$ 5-7 cm (cf. equation 3.6 and table 1).

To estimate the number of particles which sediment from the fountain fluid at the level of the floor, we compare the speed at which particles settle through the fountain fluid with the radial speed at which the fountain fluid spreads over the floor. We assume that on impinging on the floor, the fountain has a radius r_0 and a volume flux Q_{f0} (figure 8b). Mizushina *et al.* (1982) indicate that the radius of a fountain grows linearly with distance so that

$$r_0 = r_p + 0.17\left(H - \bar{h}_p\right) \tag{3.7}$$

where r_p is the radius of the fountain at a distance $H - \bar{h}_p$ above the floor (cf. equation 3.4). At the level of the floor, the volume flux of the fountain, Q_{f0}, is given by

$$Q_{f0} = k M_f^{\frac{1}{2}} \left(Q + A\bar{v}_s\right) \tag{3.8}$$

in which k is a constant of order 1 (Cooper & Hunt 2007). On reaching the base of the space the fountain fluid starts spreading radially over the floor at an initial speed

$$u_0 = \frac{Q_{f0}}{2\pi r_0 h_0} \tag{3.9}$$

in which h_0 denotes the initial depth of the spreading flow (figure 8b). Using equations 3.7 and 3.8, we estimate that in our experiments the typical radius of the descending fluid in the fountain at the level of the floor is of order $r_0 \approx$ 0.03-0.04 m, and that the typical volume flux is of order $Q_{f0} \approx 50 - 70 \cdot 10^{-6}$ m^3/s. If we assume that h_0 is of the same order as the fountain fluid radius, $h_0 = r_0 \approx$ 0.03-0.04 m (figure 8b), we obtain that the initial speed at which the fountain fluid spreads over the floor of the tank is of order $u_0 \approx 8 - 12$ mm/s, i.e. 20-30 times larger than the mean speed at which particles settle through the fluid in the tank, $\bar{v}_s$ (cf. section 2.1 and appendix A). Since $R_L \approx 2 - 3\, r_0$, we expect the mass of particles which sediment onto the floor before the fountain fluid lifts off to be small, and therefore we assume that we can use equation 3.6 to calculate the critical lift-off radius R_L.

It can be envisaged that after lifting off from the floor surface, the fountain fluid keeps propagating radially while rising through the ambient fluid in the lower part of the tank. Hence, we expect a portion of the floor area just outside the lift-off radius to be shielded and to receive a limited flux of sedimenting particles from the ambient fluid above (figure 8a). We denote the radial width of this additional area of reduced sedimentation by ΔR_L.

For $r > R_L + \Delta R_L$, we expect particles to sediment onto the floor of the tank. Consequently, the effective area over which particles sediment at the level of the floor, A_s, is

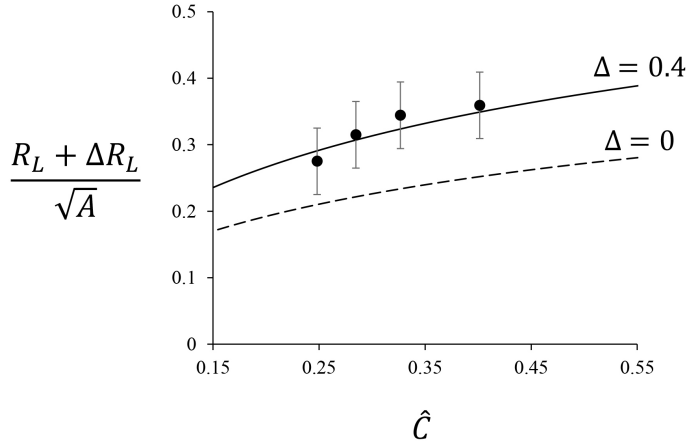

FIGURE 9. Comparison of experimental results with model predictions. For each one of the experiments listed in table 1 with $Q = 10$ cm^3/s, we measure the dimensionless concentration of particles in the ambient fluid at the base of the tank, $\hat{C}$. Based on $\hat{C}$, we calculate the fraction of the floor area over which particles do not sediment at steady state (dots). We compare the experimental results with the predictions of the model for $\Delta = 0$ (dashed line) and $\Delta = 0.4$ (solid line). Error bars of $\pm 5\%$ are plotted.

given by

$$A_s = A - \varepsilon^2 \pi^{\frac{1}{4}} \gamma^{-3} \frac{h_f^3}{H - \bar{h}_p} (1 + \Delta)^2 \tag{3.10}$$

Equation 3.10 indicates that as a result of the fountain flow the effective area over which particles sediment at the level of the floor is reduced, and so the flux of particles which sediment over the floor of the space is also reduced, and equation 2.12 should be revised to the value

$$P_{floor} = A_s \int_{D_{min}}^{D_{max}} v_s(D)\, c_b(D)\, dD \tag{3.11}$$

Thus at steady state we expect the concentration of particles in the ambient fluid at the base of the space to be given by

$$C_a = \int_{D_{min}}^{D_{max}} \frac{p_{in}(D)}{Q + A_s v_s(D)} dD \tag{3.12}$$

The model developed in sections 3.1 and 3.2 is tested in figure 9 by comparing our model predictions with experimental results. For each one of the experiments listed in table 1 with $Q = 10$ cm^3/s, we measure the dimensionless concentration of particles in the ambient fluid at a distance 2 cm from the floor of the tank, $\hat{C}$ (equation 3.2). We then use equation 3.12 to infer the effective area over which particles sediment in the tank, A_s, and the radius of the portion of the floor area over which particles do not sediment, $R_L + \Delta R_L$. We compare the results of the experiments (dots) with the predictions of the model (lines). If we assume that $\varepsilon(1 + \Delta)$ is a constant (equation 3.10), and that $\varepsilon = 0.03$ as indicated by Cooper & Hunt (2007), we observe in figure 9 that small errors of less than 2-3% are obtained for $\Delta = 0.4$ (cf. equation 3.10).

In the model we have assumed that the fountain fluid reaches the base of the tank, $h_f > H - \bar{h}_p$. This is consistent with there being a region of the floor in which sedimentation is suppressed, leading to the increase in particle concentration observed in the experiments, $C_a > C_{eq}$ (see figure 7). If there was a steady state in which the fountain did not reach

the floor of the tank, this would imply that particles can sediment over the whole floor area; therefore, the concentration of suspended particles in the ambient fluid would equal the concentration of particles in the plume fluid at the level $\bar{h}_p$ (equations 2.10 and 2.6 respectively). In this case, we would then expect that the plume fluid would descend below the level $z = \bar{h}_p$ as a neutrally-buoyant jet, and hence it would eventually reach the floor.

It should be noted that in our experiments we could only investigate the case in which $R_L^2 \ll A$. When a small flux of particles is supplied to the space, the buoyancy flux of the plume decreases and we expect the critical lift-off radius R_L to increase (equation 3.6). However, at low particle concentrations the image analysis technique used in our experiments (cf. section 2.1) becomes less accurate as the signal-to-noise ratio of the particle concentration decreases, and so we have not been able to investigate this limit quantitatively (cf. appendix B).

As noted in section 2.1, in the present paper we only consider the transport of small particles through the space. If the particles were larger, so that a significant fraction were predicted to sediment as the fountain fluid spreads over the floor, then the flow regime would become rather different. This may be seen by noting that the time to sediment through the radial flow is $\tau_s \sim h_0/\bar{v}_s$, while the time for the radial flow to reach the tank's walls is $\tau_f \sim Ah_0/Q_{f0}$, where Q_{f0} is the flux in the fountain (cf. equation 3.8). With fast sedimentation $\tau_s < \tau_f$, and so we find that $A\bar{v}_s > Q_{f0}$. This implies that particles would not be suspended by the upward return flow (equation 2.4). In this case, the particle-laden plume would descend to the base of the space and sediment particles over the floor, and the fluid vented from the space would be largely depleted of particles.

4. Plume containing particles and negatively-buoyant fluid

4.1. *Experiments*

We now introduce a second series of experiments, in which the transport of particles through a ventilated space which contains a localised source of particles and of negatively-buoyant fluid is explored (see figure 1b). Table 2 contains a list of the experiments described in this section. These experiments are performed using the same laboratory apparatus described in section 2.1 and illustrated by figure 2. In this second series of experiments, we use the same silicon carbide particles and the same image analysis technique described in section 2.1 to quantify the concentration of particles in the tank during an experiment. As in the previous experiments, fresh water is used as the ambient fluid in the tank. However, in this second group of experiments, a particle-laden solution of water and NaCl (20% in weight) is used as the plume fluid. The salinity of this solution is checked by refractometry. The saline fluid is denser than fresh water, and so it forms a turbulent, dense plume which descends through the tank while entraining ambient fluid.

For convenience, we usually start our experiments by supplying a continuous flow of saline solution which does not contain particles. This fluid is pumped into the tank through vent A (see figure 2), and forms a dense turbulent plume which descends through the tank. A ventilation flow is supplied to the tank through vent B and extracted from the tank through vent C, as described in section 2.1. Over time, the system evolves to an equilibrium, at which the fluid in the tank is stratified: the upper part of the tank contains fresh water, while the lower part of the tank contains a solution of water and salt. The two layers are separated by an interface (Linden *et al.* 1990). In our experiments, this equilibrium is usually obtained 20-30 minutes after the beginning of the experiment. Once the saline stratification is established, we add particles to the saline fluid and observe

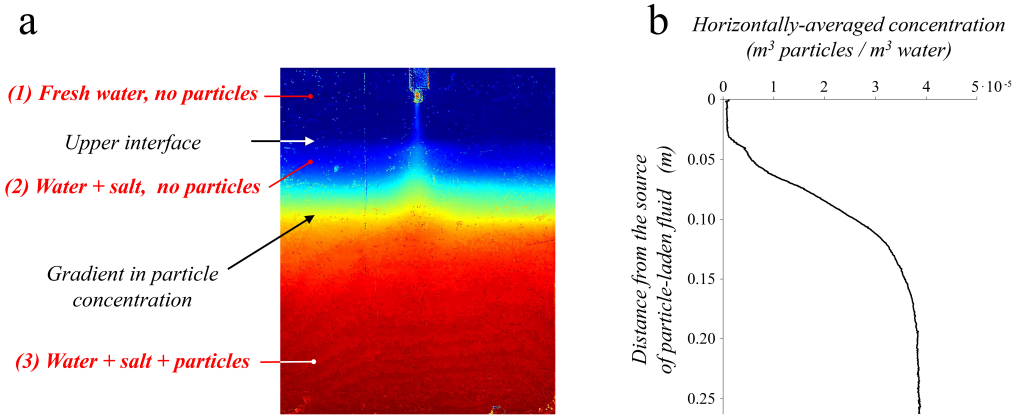

FIGURE 10. Steady-state distribution of particles in the tank in a typical experiment (experiment h, cf. table 2). Image a) illustrates the steady-state concentration of particles in the tank using false colours; image b) shows the horizontally-averaged particle concentration profile.

the transport of the particles through the tank. This experimental procedure minimises the amount of time required for the steady-state stratification of particles to develop in the tank; however, our observations indicate that the details of how an experiment approaches the steady state do not affect the steady state, and so the same steady-state distribution of particles in the tank would be obtained if both the particles and the saline fluid were supplied from the start.

Over the course of the experiment, the particle-laden plume fluid descends through the tank while entraining ambient fluid. On reaching the base of the tank, the it spreads over the floor, in an analogous fashion to that described in section 2.1. In the lower part of the tank, an upward return flow is produced in the ambient fluid, as described in section 3.1. This flow suspends particles in the ambient fluid (figure 1b). The concentration of particles in the suspension increases over time, until a steady state is reached.

At steady state, we observe that the fluid in the tank is stratified, and that three layers can be identified. The layers are characterised by different concentrations of particles and salt in the ambient fluid (figure 10). In the upper layer (layer number 1 in figure 10), the ambient fluid contains fresh water. In this layer, no particles are suspended in the ambient fluid which surrounds the plume. At the base of this layer, we observe a sharp interface which separates fresh water in the upper layer from a solution of water and salt in the lower layers in the tank. In the central part of the tank (layer number 2 in figure 10), the ambient fluid contains a solution of water and salt and a very small number of particles, which are detrained from the plume fluid at the level of the interface between layers 1 and 2 (see figure 11). In the lower part of the tank (layer number 3 in figure 10), the ambient fluid contains both salt and a large number of suspended particles. In our experiments, a continuous stratification in particle concentration is observed rather than a sharp interface between layers 2 and 3. This is the result of the distribution of grain sizes and settling speeds in the mixture of particles used for the experiments.

Over the course of a typical experiment, most of the plume fluid descends from the top of the tank to the level of the floor. However, we observe that from time to time a small amount of particle-laden fluid is detrained from the plume into the surrounding ambient at the level of the interface which separates layer 1 and layer 2 (figure 11). The concentration of particles in the ambient fluid at this level does not increase significantly during the experiment: this suggests that as new particles are intermittently detrained

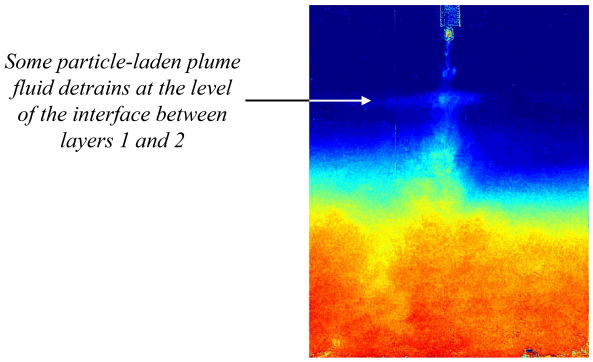

FIGURE 11. Detrainment of particle-laden plume fluid at the level of the interface between layers 1 and 2.

Experiment	$Q \cdot 10^{-6}$	$B_p \cdot 10^{-8}$	Instabilities
h	10	1.6	Yes
i	10	2.3	Yes
j	10	3.1	Yes
k	10	3.9	No
l	10	4.7	No
m	15	2.3	Yes
n	5	2.3	No

TABLE 2. List of the laboratory experiments described in section 4. In this set of experiments, the floor area of the tank and the mean settling speed of the particles are fixed at $A = 6.25 \cdot 10^{-2}$ m^2 and $\bar{v}_s = 0.40 \cdot 10^{-3}$ m/s respectively. Q (m^3/s) denotes the rate at which the ambient fluid is vented from the tank through the low-level opening and B_p ($\mathrm{m}^4/\mathrm{s}^3$) denotes the buoyancy flux associated with particles in the plume fluid. In all experiments, the buoyancy flux associated with salt in the plume fluid is fixed at $B_s = 1.45 \cdot 10^{-6}$ $\mathrm{m}^4/\mathrm{s}^3$. The last column on the right-hand side identifies the experiments in which the three-layers stratification described in section 4 is subjected to the instabilities described in section 5.

from the plume at the level of the interface, previously-detrained particles fall from the level of the interface towards the base of the tank.

We observe that in some of our experiments (cf. table 2) the three-layer stratification illustrated by figure 10 is subject to intermittent instabilities. These instabilities develop over a long time scale, and they modify the distribution of the particles in suspension in the tank for a limited amount of time. In the next sections, we first explore the three-layer stratification illustrated by figure 10, and develop a model which quantifies the height of the interface between layer 1 and layer 2, the maximum height at which particles are suspended in the ambient fluid, and the concentration of particles in the ambient fluid in layer 3. A description of the large-scale instabilities observed in some of the experiments is given in section 5.

4.2. *Three-layer stratification*

We investigate the transport of heavy, small particles through an enclosed space with downward ventilation which contains a source of heavy particles and of relatively dense fluid located at the top of the space (figure 12). We denote the negative buoyancy flux associated with the presence of particles in the plume fluid by B_p (cf. equation 2.1), and the negative buoyancy flux associated with the presence of relatively dense fluid in the

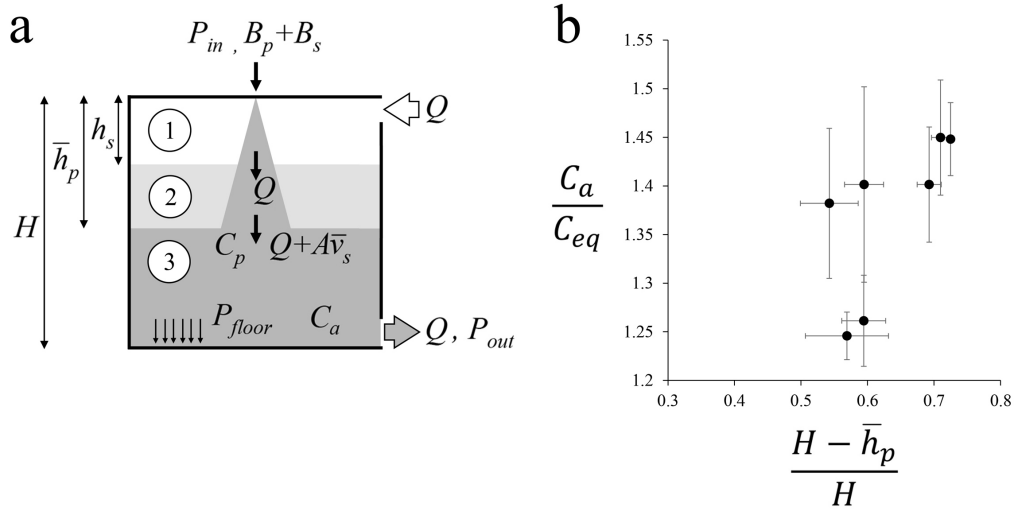

FIGURE 12. a) Cartoon showing the conditions used in the modelling (section 4); b) The measured concentration of particles at the base of the tank, C_a, is compared with the expected concentration C_{eq} given by equation 2.16.

plume by B_s. We assume that the settling speeds of the particles are small compared to the plume speed, so that the plume can be modelled as a single-phase flow (cf. sections 2 and 3).

Motivated by the experimental observations described in section 4.1, we assume that the dense, particle-laden fluid which is supplied at the top of the space produces a turbulent plume which descends through the ambient fluid in layer 1 driven by a combination of the negative buoyancy fluxes B_p and B_s. In section 4.3, we explore the entrainment of ambient fluid into the plume in this layer, and we show that at a distance h_s from the plume source an interface is formed which separates layer 1 and layer 2 (figure 12a).

Our experiments indicate that below this interface the ambient fluid is saline, and therefore its density is larger than the density of the ambient fluid in layer 1 as expected (cf. Linden *et al.* 1990). In section 4.4, we show that the particle-laden plume fluid descends through layer 2 driven by negative buoyancy flux B_p. In this layer, a return flow is produced in the ambient fluid which surrounds the plume. In the lower part of the space, particles are suspended by this flow and form a layer of particle-laden fluid (layer 3 in figure 12a, cf. section 2.4).

Using the same approach described in section 2.4, for each one of the experiments listed in table 2 we use equation 2.16 to calculate the mean concentration of particles in the ambient fluid, C_{eq}, at which the flux of particles supplied to the space, P_{in}, is balanced at steady state by the combination of the flux of particles which are vented from the space, P_{out}, and the flux of particles which sediment over the entire floor area, P_{floor} (see figure 12a and equations 2.11 and 2.12). In figure 12b we compare this concentration with the effective concentration C_a which we measured at the base of the tank in each experiment (see figure 7). Figure 12b shows that in all our experiments the measured concentration at the base of the tank exceeds the concentration given by equation 2.16 by 25-45%. As described in section 3, we therefore expect the particle-laden plume to transform into a momentum-driven fountain in layer 3. We explore the behaviour of the fountain fluid in section 4.5.

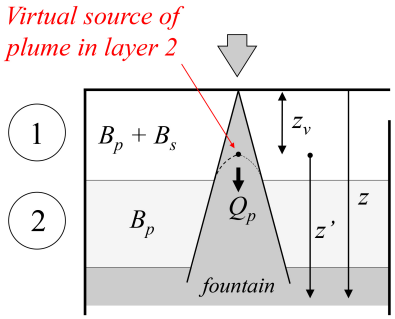

FIGURE 13. Virtual source of the particle-laden plume which descends through layer 2.

4.3. *Plume containing particles and dense fluid in layer 1*

In the upper layer the plume fluid has a negative buoyancy flux $B_s + B_p$ relative to the ambient fluid (cf. table 2). The plume entrains ambient fluid while descending through the layer. Plume theory indicates that the volume flux at a distance z from the source is given by (Linden *et al.* 1990)

$$Q_p(z) = \lambda \left(B_p + B_s\right)^{\frac{1}{3}} z^{\frac{5}{3}} \tag{4.1}$$

When the plume volume flux equals the ventilation flux, $Q_p(z) = Q$, all of the ventilation flow has been entrained by the plume and so the ambient fluid which surrounds the plume is not subject to any vertical motion (Linden *et al.* 1990). At this level, an interface is formed, which separates layer 1 and layer 2 (see figure 12a). The vertical distance between the plume source and this interface is given by

$$h_s = \frac{Q^{\frac{3}{5}}}{\lambda^{\frac{3}{5}} \left(B_p + B_s\right)^{\frac{1}{5}}} \tag{4.2}$$

At the level of this upper interface, the plume has a radius r_s (Morton *et al.* 1956)

$$r_s = \frac{6}{5}\alpha h_s \tag{4.3}$$

so that the momentum flux of the plume fluid at the level of the upper interface, M_s, is given by

$$M_s = \frac{Q^2}{\pi r_s^2} \tag{4.4}$$

4.4. *Plume containing particles in layer 2*

On crossing the interface between layers 1 and 2, the plume fluid experiences a change in the density of the surrounding fluid. The density difference between the ambient fluid in layer 1 and the ambient fluid in layer 2 is associated with the change in salinity, and can be given in terms of the reduced gravity, g_2' (Linden *et al.* 1990)

$$g_2' = \frac{B_s}{Q} \tag{4.5}$$

Plume theory indicates that at the level of the interface, the time-averaged mean salinity of the plume fluid equals that of the ambient fluid below the interface. However, the plume fluid contains particles, and so the bulk density of the plume fluid is larger than

the density of the ambient fluid in layer 2, and the mean negative buoyancy flux of the plume in this layer is given by B_p (figure 13). It is worth noting that in practice, during our experiments plumes are effectively composed of transient or intermittent eddies. It can be envisaged that as a result of the entrainment of ambient fluid in layer 1, these eddies may have a range of salinities. Hence, it is likely that from time to time a certain amount of plume fluid might be slightly less dense than the surrounding ambient fluid in layer 2. When this happens, the plume fluid detrains just below the interface between layer 1 and layer 2, as illustrated by figure 11. It can be envisaged that the presence of particles in the plume fluid may change the frequency of such detrainment events. Since the ambient fluid in layer 2 does not contain particles, the detrainment events will be more frequent when the plume fluid contains a small concentration of particles.

Cooper & Linden (1996) explored how the properties of a plume change when the plume crosses a density interface and enters a layer of fluid in which its buoyancy is reduced. Using their approach, we assume that the particle-laden plume which descends through layer 2 with reduced negative buoyancy flux B_p originates from a virtual source of finite momentum flux but zero volume flux (figure 13). This virtual source is located above the interface between layers 1 and 2, at a distance $z_v < h_s$ from the top of the space (Cooper & Linden 1996)

$$z_v = \left(\frac{Q^3}{20\pi^2\alpha^4 B_p}\right)^{\frac{1}{5}} \left(\frac{1-\hat{B}}{\hat{B}}\right)^{\frac{3}{10}} \int_0^{\left(\frac{\hat{B}}{1-\hat{B}}\right)^{\frac{1}{2}}} \frac{dt}{(1+t^2)^{\frac{1}{5}}} \tag{4.6}$$

in which

$$\hat{B} = \frac{B_p}{B_p + B_s} \tag{4.7}$$

is the ratio between the plume buoyancy flux below the level of the interface which separates layer 1 and layer 2 and the plume buoyancy flux above the level of that interface. In our experiments, this ratio is typically of order $\hat{B} \approx 10^{-2}$, so that the virtual origin of the particle-laden plume which descends through layer 2 is typically located 2-3 cm above the interface which separates layer 1 and layer 2.

As the particle-laden plume descends through layer 2, it entrains ambient fluid in this layer. The volume flux in the plume at a distance z' from the virtual source (see figure 13) is given by (Cooper & Linden 1996)

$$\frac{dQ_p}{dz'} = 2\pi\alpha \left[\frac{5}{8}\frac{B_p Q_p^2}{\pi^3\alpha} + \left(1-\hat{B}\right) M_s^{\frac{5}{2}}\right]^{\frac{1}{5}} \tag{4.8}$$

Equation 4.8 is solved numerically, using $Q_p\left(z' = h_s - z_v\right) = Q$ as a boundary condition, to calculate the plume volume flux at different levels in layer 2. This volume flux is larger than the ventilation flux, so a return flow is generated in the ambient fluid which surrounds the plume in layer 2. The mean speed at which the ambient fluid rises through the space, $v_w(z')$, is calculated using a combination of equations 2.3 and 4.8. When this speed equals the speed at which a particle settles through the ambient fluid, v_s, the particle becomes suspended in the ambient fluid. As a result of the distribution of settling speeds in the mixture of particles used in the experiments, a continuous stratification in particle concentration develops in the lower part of the space (cf. section 2.3). We denote the vertical distance between the source of the plume and the level at which particles with a mean settling speed $\bar{v}_s$ are suspended in the ambient fluid by $\bar{h}_p$.

We use the model developed in sections 4.2-4.4 to calculate the distance between the

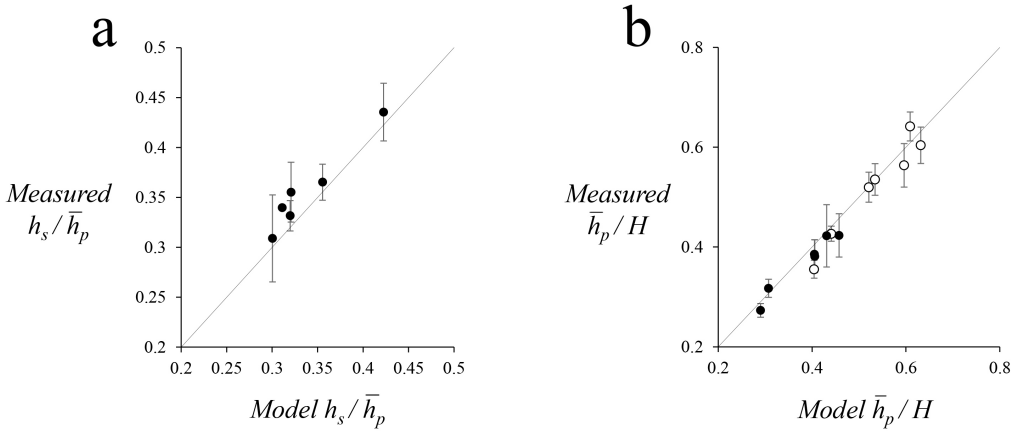

FIGURE 14. Comparison of experimental results with model predictions: a) distance between the plume source and the interface between layer 1 and layer 2, h_s; b) distance between the plume source and the level at which particles with a mean settling speed $\bar{v}_s$ are suspended in the ambient fluid, $\bar{h}_p$.

plume source and the interface between layer 1 and layer 2, h_s, and the distance between the plume source and the level at which particles with a mean settling speed $\bar{v}_s$ are suspended in the ambient fluid, $\bar{h}_p$. In figure 14a we consider the vertical distance between the source of the plume and the interface between layers 1 and 2, h_s: for each one of the experiments listed in table 2, we compare the distance predicted by the model (equation 4.2) with the distance which we measured during the experiment (black dots). In figure 14b we consider the distance between the source of the plume and the level at which particles with a mean settling speed are suspended in the ambient fluid, $\bar{h}_p$. For each experiment, we solve equation 4.8 numerically, and calculate the height at which $Q_p = Q + A\bar{v}_s$ (cf. equation 2.4). We then compare this height with the height at which the concentration of particles in the ambient fluid is reduced by 50% relative to the maximum concentration which we measure at the base of the tank (black dots). For comparison, in figure 14b, we also plot the results of the experiments described in section 2.1 (plume containing particles and neutrally-buoyant fluid) using white dots. Both figures 14a and b show that there is a relatively good agreement between model predictions and experimental observations, with errors of less than 3-5% in most experiments.

4.5. *Fountain in layer 3*

Motivated by the experimental results illustrated by figure 12b, we use the same approach described in section 3 and assume that the particle-laden fluid transitions into a fountain at the level at which particles with a mean settling speed $\bar{v}_s$ are suspended in the ambient fluid. We assume that at this level $z = \bar{h}_p$ the particle-laden plume fluid has an upward buoyancy flux B_f relative to the surrounding ambient fluid (equation 3.1) and a momentum flux M_f (equation 3.3). In our experiments the fountain fluid reaches the base of the space and propagates radially over the floor until it separates from the surface of the floor at a distance R_L from the plume vertical axis (cf. equation 3.6 and figure 8a). As described in section 3.2, the radial speed at which the fountain fluid spreads over the floor is large compared with the mean particle settling speed in our experiments, and so we expect the sedimentation of particles to be suppressed for $r < R_L$. After lifting off from the floor surface, the fountain fluid propagates radially while rising through the ambient fluid (figure 8a). Consequently, we expect a portion of the floor area just outside

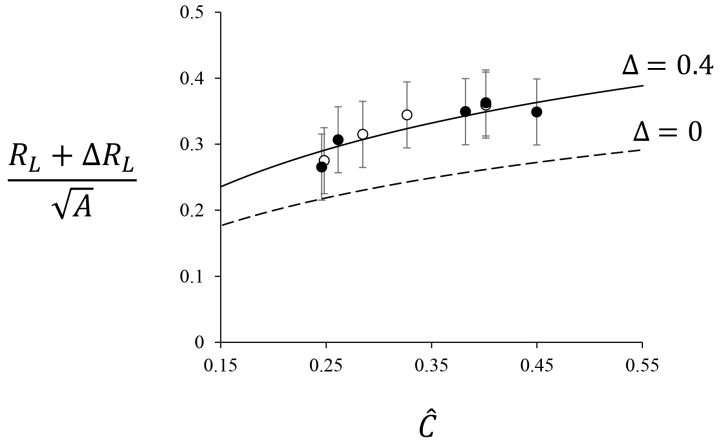

FIGURE 15. Comparison of experimental results with model predictions. For each one of the experiments listed in table 2 with $Q = 10$ cm^3/s, we measure the dimensionless concentration of particles in the ambient fluid at the base of the tank, $\hat{C}$. Based on $\hat{C}$, we calculate the fraction of the floor area over which particles do not sediment at steady state (black dots). We compare the experimental results with the predictions of the model for $\Delta = 0$ (dashed line) and $\Delta = 0.4$ (solid line). The outcomes of the experiments described in section 2.1 are plotted for comparison (white dots, compare with figure 9). Error bars of $\pm 5\%$ are added to the graph.

the lift-off radius R_L to be shielded and to receive a limited flux of sedimenting particles from the ambient fluid above. We denote the radial width of this additional area of reduced sedimentation by ΔR_L, and based on the experimental results described in section 3.2 we expect $\Delta \approx 0.4$.

In figure 15, the model developed in sections 4.3-4.5 is tested by comparing the results of our experiments with the prediction of the model. Using the same approach described in section 3.2, for each one of the experiments listed in table 2 with $Q = 10$ cm^3/s we measure the dimensionless concentration of particles in the ambient fluid at the base of the tank, $\hat{C}$. We then use equation 3.10 to infer the fraction of the floor area over which particles sediment effectively and the radius of the portion of the floor area over which particles do not sediment, $R_L + \Delta R_L$. We compare the results of the experiments (black dots in figure 15) with the prediction of the model developed in sections 4.3-4.5 (lines). Figure 15 shows that for $\Delta = 0.4$ the model prediction lies within 5% of the experimental data for all measurements. Similar errors were obtained when analysing the results of the experiments described in section 2.1 (white dots, which are plotted in figure 15 for comparison).

5. Instabilities

In some of our experiments (cf. table 2) the three-layer stratification described in section 4 is subject to intermittent instabilities. Figure 16 shows how the horizontally-averaged mean concentration of particles at different levels in the tank changes over time in two experiments (k and h, cf. table 2). The figure shows that in experiment k, which is characterised by a relatively large particle buoyancy flux B_p (cf. table 2), the three-layer stratification described in section 4 is stable: we observe that in the upper part of the tank the ambient fluid does not contain particles (dark blue colour in the false-colour image), while the concentration of particles is maximised in the lower part of the tank (red colour in the false-colour image). At the level of the interface between layer 1 and

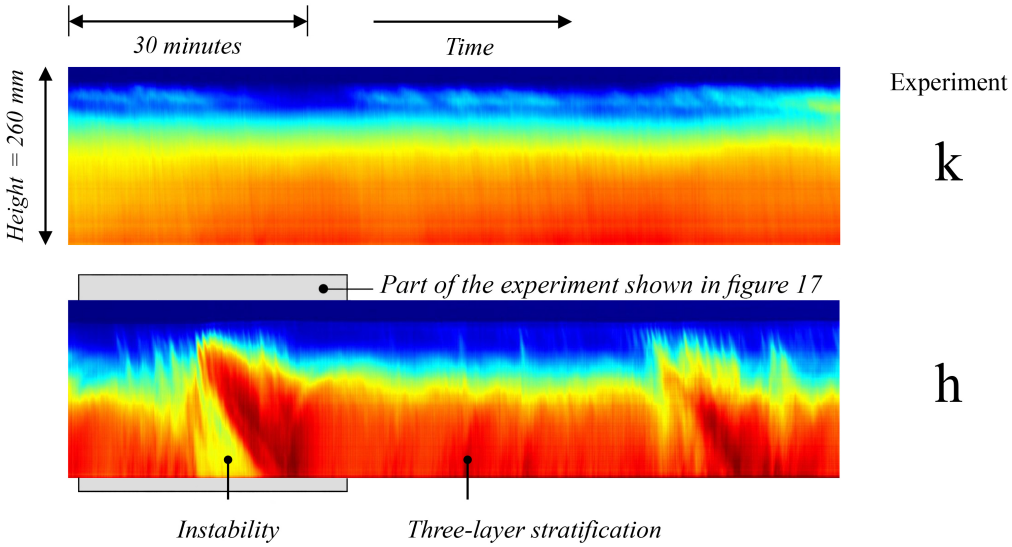

FIGURE 16. Transient horizontally-averaged mean concentration of particles in the tank in experiments k and h (cf. table 2). In experiment k, a steady three-layer stratification is observed (cf. section 4). In experiment h, we observe intermittent instabilities.

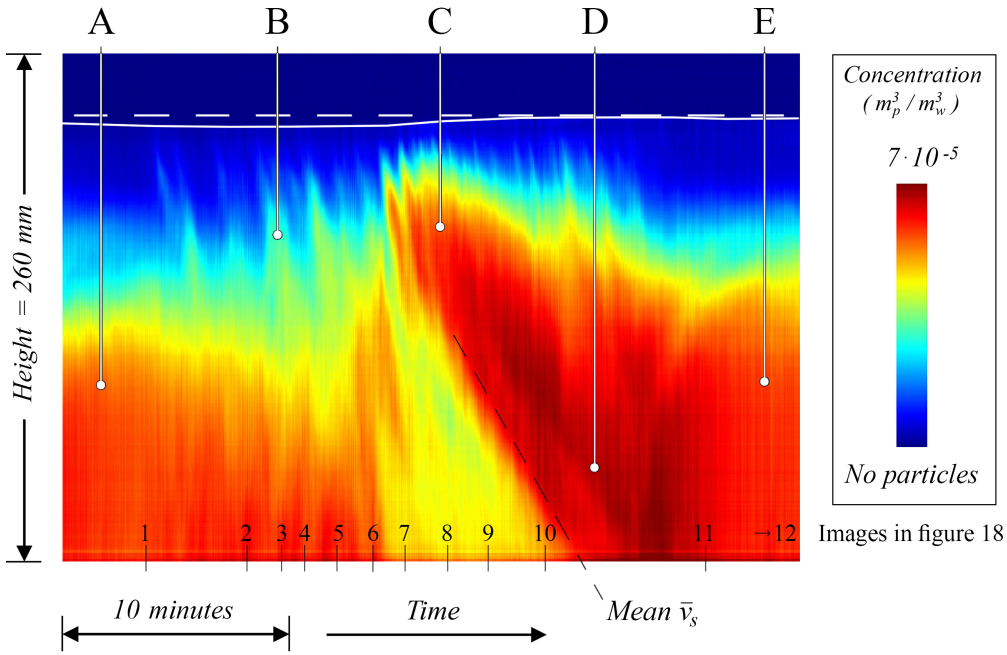

FIGURE 17. This figure illustrates how the horizontally-averaged mean concentration of particles in the tank changes during one of the instabilities which develop in experiment h. The part of the experiment illustrated in this figure has been highlighted in figure 16. In this figure, the vertical position of the interface between layers 1 and 2 is highlighted using a white continuous line. A reference horizontal dashed line is plotted for comparison.

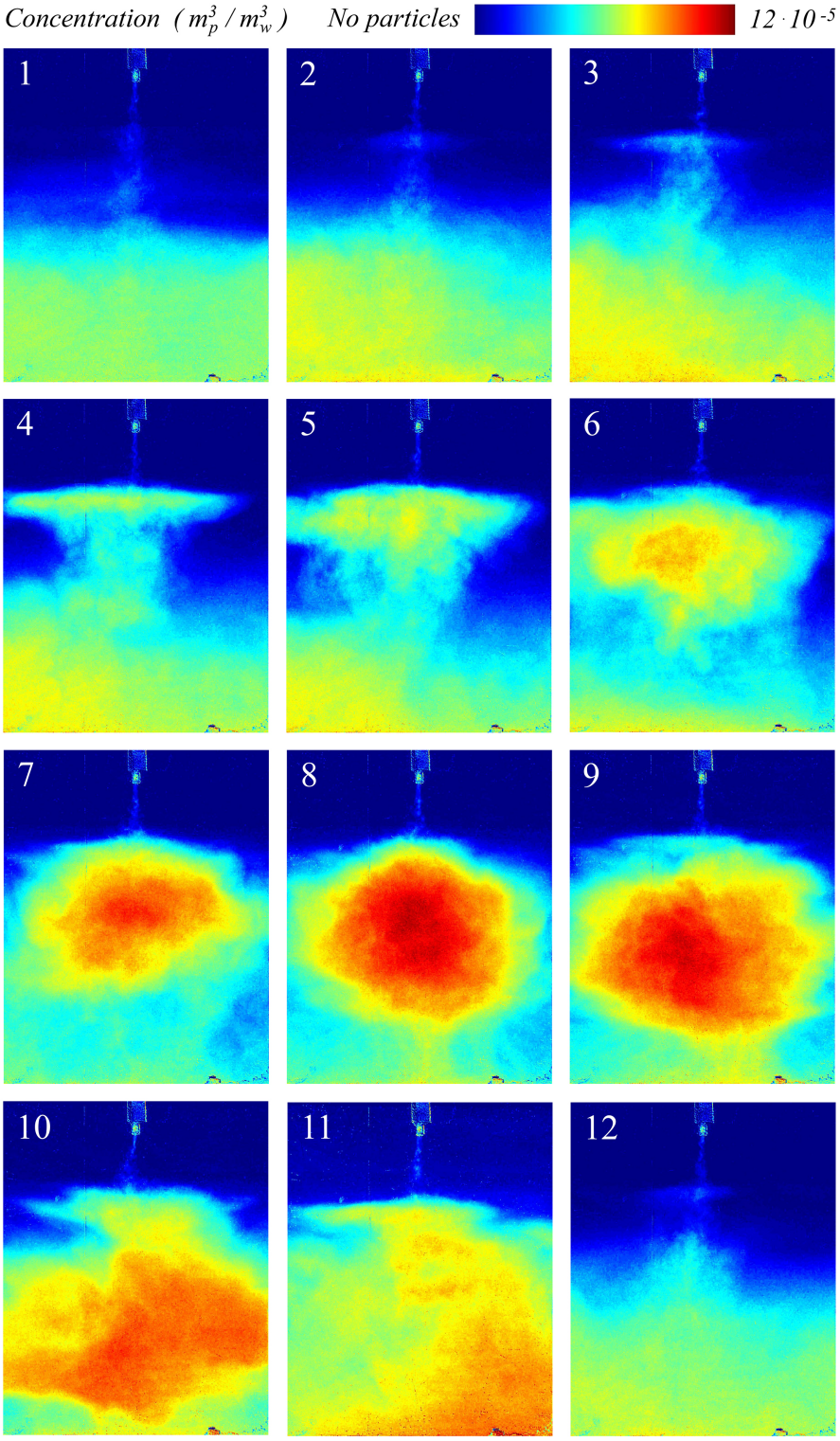

FIGURE 18. Large-scale instability observed during experiment h. Image 1 was captured 670 seconds after particles were added to the plume fluid at the beginning of the experiment. Images 2-12 were captured at the following times (relative to image 1): 220, 296, 352, 414, 490, 558, 652, 738, 862, 1212 and 1544 seconds.

layer 2, we observe that a small flux of particle-laden fluid is detrained from the plume. This produces a small, unsteady increase in the concentration of particles in layer 2, but does not affect the three-layer stratification of the space.

However, figure 16 shows that in experiment h, which is characterised by a relatively small particle buoyancy flux B_p (cf. table 2), the three-layer stratification is subject to large-scale, intermittent instabilities. We focus on one of these instabilities, and observe how the concentration of particles in the ambient fluid changes during the instability. In figure 17, we zoom in on a portion of figure 16, and observe how the horizontally-averaged mean concentration of particles in the tank changes over the course of a limited time interval during which the instability develops. In figure 18, the distribution of particles in the tank is shown at different times during the same instability to help illustrate the nature of the instability. Over the course of the instability, we observe that the height of the interface which separates layer 1 and layer 2 is subject to a small oscillation. We use a thin solid white line in figure 17 to illustrate how the height of the interface changes over time. A reference horizontal dashed line is plotted in the same image for comparison.

Figure 17 (letter A) and image 1 in figure 18 show that before the beginning of the instability, the fluid in the tank is stratified in particles. The three-layer stratification is maintained for several minutes (image 2 in figure 18). During this time, we observe that the interface between layers 1 and 2 is located 2-3 millimetres below its steady-state level, given by equation 4.2. As a result of this perturbation in the interface height, the plume entrains a larger amount of fresh water in the upper layer; consequently, on crossing the interface between layers 1 and 2 the plume fluid is slightly less dense than the ambient fluid below the interface. As a result of this density difference, a flux of particle-laden fluid is detrained from the plume into the ambient below the interface between layers 1 and 2 (image 3 in figure 18).

If the perturbation in the height of the interface between layer 1 and layer 2 persists for a sufficiently long time, a flux of particle-laden plume fluid is continuously detrained in layer 2. Consequently, the concentration of particles in this layer increases. When the concentration becomes sufficiently large, some of the particles in the layer descend towards the base of the tank by convective sedimentation (figure 17, letter B). Eventually, the bulk density of the ambient fluid in layer 2 becomes large enough that a large fraction of the plume fluid is detrained at the level of the interface between layer 1 and layer 2 (images 4-6 in figure 18).

When this happens, a major change in the distribution of particles in the tank occurs. The concentration of particles in layer 2 increases, because a large flux of particles is transported into this layer by the plume (letter C in figure 17 and images 5 and 6 in figure 18). However, the concentration of particles in the lower part of the tank, which is now deprived of a source of new particles from the plume, decreases. As the plume fluid is increasingly detrained at the level of the upper interface, the return flow in the ambient fluid in layer 3 is reduced. Consequently, particles in this layer are no longer suspended by the upward motion of the ambient fluid described in section 2.4, and they gradually settle through the ambient fluid and sediment onto the floor (images 4-6 in figure 18).

Figure 16 shows that the fluid in the tank remains unstably stratified in particle concentration for approximately 10-15 minutes. During this time, a growing region of fluid containing a high concentration of particles (images 7-10 in figure 18) descends from the central part of the tank (layer 2) towards the base of the tank at a speed comparable with the mean settling speed of the particles, $\bar{v}_s$ (see figure 17). A flux of new particles is continuously supplied to this region of particle-laden fluid by the plume, so the concentration increases over time. In our experiments, this concentration exceeds the

steady-state concentration of particles in the ambient fluid at the base of the tank, C_a (see figure 17 and images 7-9 in figure 18).

Eventually, the region of particle-laden fluid reaches the floor of the tank, over which particles sediment (letter D in figure 17 and images 10-11 in figure 18). At this point, the plume again descends to the base of the space and a new three-layer stratification is gradually built, starting from the bottom of the tank (letter E in figure 17 and image 12 in figure 18). The ambient fluid in the tank remains stably stratified in particle concentration until a new instability occurs, several minutes after the end of the previous one (see figure 16).

In our experiments, we observed several instabilities similar to that described above. These instabilities did not develop at regular time intervals, and we could not identify the specific conditions which triggered the initial perturbation in the height of the interface between layer 1 and layer 2. However, we observed that the time lapse between two instabilities was frequently of order 30-40 minutes (see figure 16). This time scale is comparable with the filling box time scale for a tank of dimensions 25 x 25 x 25 cm (approximate volume of layers 2 and 3) ventilated at a rate $Q = 10$ cm^3/s (cf. table 2).

Among our experiments, those with a relatively large particle buoyancy flux B_p did not develop any instability; while those with a smaller B_p became unstable (cf. table 2). It may be envisaged that when the density of the fluid in the plume is reduced slightly as a result of a perturbation in the height of the interface between layer 1 and layer 2, a sufficiently small concentration of particles in the plume fluid is required for the plume fluid to become relatively buoyant compared with the surrounding ambient fluid in layer 2. In this case, the plume fluid detrains in the central layer, and the system becomes unstable. If, however, the concentration of particles in the plume fluid is large, the plume fluid remains relatively dense compared with the surrounding ambient fluid and descends through layer 2. In this case the system does not become unstable.

It would be interesting to develop a more detailed understanding of the dynamics of these instabilities, but this is beyond the scope of the present paper and may be the subject of future studies.

6. Conclusions

We have explored the transport of small, heavy particles through an enclosed space which contains a localised source of particle-laden fluid at high level. A background flow of ambient fluid which does not contain particles is supplied to the space at high level, and an equivalent amount of fluid is extracted from the space at low level. The bulk density of the particle-laden fluid is larger than the density of the ambient fluid, which does not contain particles. As a result of this density difference, the particle-laden fluid forms a turbulent plume which descends through the space while entraining ambient fluid.

New laboratory experiments have shown that as a result of plume entrainment, a return flow is produced in the ambient fluid which surrounds the plume in the lower part of the space. When the upward speed of the ambient fluid equals the fall speed of a particle, the particle becomes suspended in the ambient fluid. The vertical distance h_p between the plume source and the maximum height at which a particle with a settling speed v_s is suspended in the ambient fluid is controlled by the rate of ventilation of the space, the speed at which particles fall through the fluid, and the cross-sectional area of the space (equation 2.5). However, h_p is not controlled by the height of the space; consequently, the depth of the region in which particles are suspended in the ambient fluid increases when the height of the space is increased.

Our laboratory experiments have shown that on entering the layer of particle-laden fluid at the base of the space, the plume fluid contains fewer particles than the surrounding ambient fluid. Consequently, the plume fluid becomes relatively buoyant and transitions into a momentum-driven fountain. In our experiments the maximum height travelled by the fountain fluid through the particle-laden ambient fluid, h_f, exceeds the mean depth of the layer of particle-laden fluid, $H - \bar{h}_p$, and so the fountain impinges on the floor of the space. In this case, the fountain fluid spreads radially over the floor until it reaches a critical distance from the fountain vertical axis, R_L (equation 3.6), at which it separates from the floor surface and lifts off due to its upward buoyancy. In this paper we have focused on the case $R_L^2 \ll A$, and we have observed that in this case if the speed at which the fountain fluid spreads radially at the level of the floor is sufficiently large, particle sedimentation is reduced for $r < R_L$. Hence, particles in the ambient fluid can only sediment onto a fraction of the floor area, A_s (equation 3.10). The reduction in the area over which particles effectively sediment onto the floor results in an increase in the concentration of particles in the ambient fluid below the interface (equation 3.12), and in an increase in the flux of particles which are vented from the space at steady state (equation 2.11).

When a flow of relatively dense fluid containing particles is supplied at the top of a downward-ventilated space, a three-layer stratification develops in the space at steady state: the upper layer (layer 1) contains relatively low-density ambient fluid in which no particles are suspended; the central layer (layer 2) contains a denser mixture of ambient and plume fluid in which no particles are suspended; and the lower layer (layer 3) contains a suspension of particles in the same mixture of ambient and plume fluid. The particle-laden, relatively dense fluid which is supplied at the top of the space forms a turbulent plume which descends through layers 1 and 2. On entering layer 3, the plume fluid becomes relatively buoyant relative to the surrounding ambient fluid, and transitions into a momentum-driven fountain. The fountain fluid descends through the ambient fluid in layer 3, spreads radially over the floor and produces an area over which particle sedimentation is reduced or suppressed. As a result, the concentration of particles in the ambient fluid in layer 3 and the fraction of particles which are vented from the space at steady state increase.

We have observed that the described three-layer stratification can be subject to large scale, intermittent instabilities. These instabilities appear to be originated by small perturbations in the height of the interface between layers 1 and 2. When the distance between the plume source and this interface is increased, the plume entrains more ambient fluid through layer 1. Consequently, the bulk density of the plume fluid is reduced at the level of the interface which separates layer 1 and layer 2, and some of the plume fluid is detrained into the ambient fluid in layer 2. This results in an increase in the concentration of particles in this layer, and in a reduction in the concentration of particles in layer 3. Over the course of an instability, a region of fluid with a high concentration of particles is formed in layer 2, and gradually settles through the space, until it reaches the floor on which particles sediment. Eventually, a new three-layer stratification is developed in the space.

The fundamental outcomes described in this paper can be used to help inform a range of different problems, including the transport of contaminants through a space with downward displacement ventilation (see figure 1). In buildings, particulate contaminants are frequently produced and can be airborne carriers for various pathogens (Noakes *et al.* 2012). The diameter of these particles can change, but is frequently of order 5-15 μm (Gralton *et al.* 2011), and so the smaller contaminants settle through air at a low speed of order 1 mm/s (Chao *et al.* 2009). In a warm climate or season, a flux of cold air may

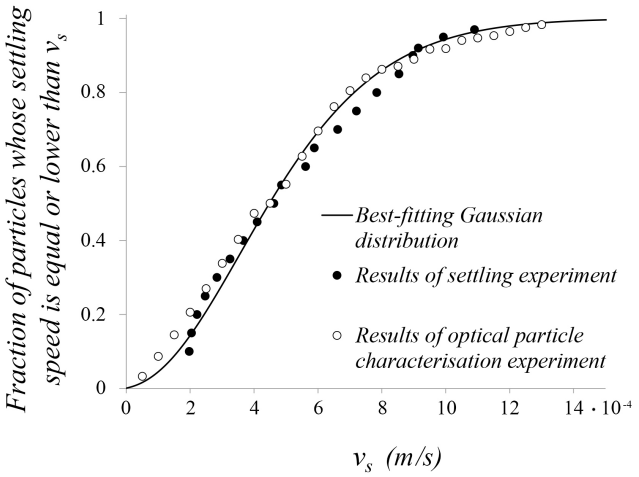

FIGURE 19. Distribution of settling speeds in the mixture of particles used in the experiments.

be supplied at high level to a room with downward ventilation (Chenvidyakarn & Woods 2005). To provide thermal comfort to occupants, this flux of cold air will be adjusted so that the interface which separates the warm air in the upper part of the room from the colder air in the lower part of the room is sufficiently tall, say $H - h_s \approx 3$ m (cf. equation 4.2). Our model indicates that if a small flux of particulate contaminants are released at the source of the cold air, a layer of contaminated ambient air is formed at the base of the room. We denote the depth of this layer above the floor by $H - h_p$ (cf. equation 2.5), and use the model developed in section 4 to estimate this depth. We assume that the room is of a typical floor area $A = 30$ m^2 and of a typical height $H = 4$ m. The room contains 3-5 occupants and is ventilated at a rate $Q = 10$ litres per second per occupant (CIBSE 2007). In these conditions, our model indicates that for $v_s = 1$ mm/s, the vertical distance between the upper and the lower interface is of order $h_s - h_p \approx 0.3$-0.5 m, and so the depth of the layer of contaminated air in the room is approximately $H - h_p \approx$ 2.5-2.7 m. This simple calculation indicates that for particles with a small settling speed such as those frequently found in buildings, a large fraction of the thermally-comfortable air in a room with downward displacement ventilation may also be contaminated if the source of cold air at the top of the room releases particles. Equation 2.5 indicates that the depth of the layer which contains contaminated air will be larger when the floor area A is small or when the height of the room H is large.

Acknowledgements

This work has been funded through the BP Institute, EPSRC and Hughes Hall, Cambridge. We gratefully acknowledge the technical assistance of A. Pluck, and the constructive comments of Professor C. Noakes, Dr. C. P. Caulfield and of three anonymous referees.

Appendix A. Distribution of settling speeds in the mixture of particles used in the experiments

A settling experiment was performed to measure the distribution of settling speeds in the mixture of particles used in the experiments. In this experiment, the tank was

initially filled with a suspension of water and particles at a known concentration. The transient settling of the particles was monitored. The black dots in figure 19 illustrate the results of this experiment. As an independent test, we also ran an optical particle characterisation experiment using a Malvern Morphologi image analyser. In this experiment, the equivalent spherical diameters of approximately 40,000 particles were measured. For each one of these particles, we inferred the associated settling speed using Stoke's law. We calculated the statistical distribution of the settling speeds, and plotted the results in figure 19 using white dots. Based on the results of both experiments, we calculated the best-fitting Gaussian distributions of settling speeds (solid curve in figure 19), which has been used in the paper.

Appendix B. Image analysis technique used in the experiments

During our experiments, an electroluminescent LightTape (Electro-LuminX Lighting Corp.) was connected to the rear of the tank. The light produced by this light sheet was transmitted through the tank and captured by a computer-controlled Nikon D90 RGB DSLR camera on the opposite side. The camera was located at a distance 3 m from the front of the tank. We took photographs at regular time intervals, with a frequency ranging between 0.5 and 4 Hz. The shutter speed was 1/15 s, and we used ISO 800 to take images with an 80 mm lens. This provided a fast shutter speed to approximate an instantaneous capture of the flow dynamics in the tank.

Because of their small diameter, individual particles could not be identified in the photographs. However, different concentrations of particles in the tank resulted in different levels of light attenuation through the tank, which were captured by the camera.

To convert a photograph into a matrix describing the concentration distribution in the tank, we used a set of calibration images. Before the beginning of each experiment, we prepared 20-25 suspensions of particles in water. We filled in the tank with each suspension and stirred vigorously, leading to a virtually uniform distribution of particles in the tank. For each suspension, we took 30 calibration photographs of the tank. We then subdivided each of these images into cells of dimensions 4 x 4 pixels, and we determined the average light intensity in every one of these cells for each suspension. Finally, we obtained an empirical calibration curve for each cell using a linear interpolation between the recorded averages. Using this approach, a total of 350 x 400 calibration curves were generated to convert the light intensity field into a concentration distribution field.

We tested the calibration by adding a known amount of particles in the tank containing clear water, and by comparing the mass of particles detected using the image-analysis technique with the known mass of particles supplied to the tank. These tests showed that using our experimental technique the mass of particles was conserved in the tank, with errors of approximately 2-5%.

Over the course of each experiment, very small changes in the ambient conditions or in the brightness of the light sheet which is located behind the tank produced a background noise in the data. In our experiments the concentration of particles in the tank was always sufficiently large that the errors associated with such disturbances were very small (of order 1%). However, it should be noted that if the number of particles which are suspended in the ambient fluid is reduced, the attenuation of light through the tank is also reduced, and so the signal-to-noise ratio of the particle concentration decreases. For this reason, we could not explore the limit of very small buoyancy fluxes B_p using the described experimental technique, as noted in section 3.2.

To conclude, we would like to underline that we only used the image analysis technique to quantify the line-of-sight average concentration of particles at different levels

in the tank (see figures 3, 4, and 10, and note that in our experiments particles are approximately well-mixed horizontally in the tank at steady state). However, additional calibration of the experimental technique would be required to quantify the concentration of particles in a localised region of fluid in the tank (e.g., the concentration of particles in the plume fluid, which is located in the centre of the tank and is surrounded by a certain volume of ambient fluid at a different concentration) or the transient concentration of particles in the tank (see the images on the left-hand side of figure 3, and note that particles are not always well-mixed horizontally in the tank at the beginning of the experiment).

REFERENCES

Atkinson, J., Chartier, Y., Pessoa-Silva, C. L., Jensen, P., Li, Y. & Seto, W. 2009 *Natural Ventilation for Infection Control in Health-Care Settings*. WHO Publications.

Bloomfield, L. J. & Kerr, R. C. 1998 Turbulent fountains in a stratified fluid. *J. Fluid Mech.* **358**, 335–356.

Bloomfield, L. J. & Kerr, R. C. 2000 A theoretical model of a turbulent fountain. *J. Fluid Mech.* **424**, 197–216.

Bower, D. J., Caulfield, C. P., Fitzgerald, S. D. & Woods, A. W. 2008 Transient ventilation dynamics following a change in strength of a point source of heat. *J. Fluid Mech.* **614**, 15–37.

Burridge, H. C. & Hunt, G. R. 2012 The rise heights of low- and high-froude-number turbulent axisymmetric fountains. *J. Fluid Mech.* **691**, 392–416.

Chao, C. Y. H., Wan, M. P., Morawska, L., Johnson, G. R., Ristovski, Z. D., Hargreaves, M., Mengersen, K., Corbett, S., Li, Y., Xie, X. & Katoshevski, D. 2009 Characterization of expiration air jets and droplet size distributions immediately at the mouth opening. *Aerosol Science* **40**, 122–133.

Chenvidyakarn, T. & Woods, A. W. 2005 Top-down precooled natural ventilation. *Building Services Engineering Research and Technology* **26**, 181–193.

CIBSE 2007 *Environmental Design, Guide A*. CIBSE Publications.

Cooper, P. & Hunt, G. R. 2004 Experimental investigation of impinging axisymmetric turbulent fountains. *Proceedings of the 15th Australian Fluid Mechanics Conference* .

Cooper, P. & Hunt, G. R. 2007 Impinging axisymmetric turbulent fountains. *Physics of Fluids* **19**, 117101–117101–9.

Cooper, P. & Linden, P. F. 1996 Natural ventilation of an enclosure containing two buoyancy sources. *J. Fluid Mech.* **311**, 153–176.

Frank, J. & Prost, J. 2009 Generic theory of colloidal transport. *The European Physical Journal E: Soft Matter and Biological Physics* **29.1**, 27–36.

Gladstone, C. & Woods, A. W. 2001 On buoyancy-driven natural ventilation of a room with a heated floor. *J. Fluid Mech.* **441**, 293–314.

Gralton, J., Tovey, E., McLaws, M. L. & Rawlinson, W. D. 2011 The role of particle size in aerosolised pathogen transmission: A review. *Journal of Infection* **62**, 1–13.

Kuesters, A. S. & Woods, A. W. 2011 The formation and evolution of stratification during transient mixing ventilation. *J. Fluid Mech.* **670**, 66–84.

Linden, P., Lane-Serff, G. F. & Smeed, D. A. 1990 Emtying filling boxes: the fluid mechanics of natural ventilation. *J. Fluid Mech.* **212**, 309–335.

Martin, D. & Nokes, R. 1989 A fluid-dynamical study of crystal settling in convecting magmas. *Journal of Petrology* **30**, 1471–1500.

Mingotti, N. & Woods, A. W. 2015 On the transport of heavy particles through an upward displacement-ventilated space. *Under consideration for publication in J. Fluid Mech.* .

Mizushina, T., Ogino, F., Takeuchi, H. & Ikawa, H. 1982 An experimental study of vertical turbulent jet with negative buoyancy. *Warme-und Stoffubertragung* **16**, 15–21.

Morton, B. R., Taylor, G. & Turner, J. S. 1956 Turbulent gravitational convection from maintained and instantaneous sources. *Proc. R. Soc. Lond. A* **234**, 1–23.

Nienow, A. W., Edwards, M. F. & Harnby, N. 1997 *Mixing in the Process Industries*. Butterworth-Heinemann.

Noakes, C. J., Sleigh, P. A. & Khan, A. 2012 Appraising healthcare ventilation design from combined infection control and energy perspectives. *HVAC&R Research* **18**, 658–670.

Phillips, J. C. & Woods, A. W. 2001 Bubble plumes generated during recharge of basaltic magma reservoirs. *Earth and Planetary Science Letters* **186**, 297–309.

Turner, J. S. 1966 Jets and plumes with negative or reversing buoyancy. *J. Fluid Mech.* **26**, 779–792.

Werther, J. 2007 *Fluidized Bed Reactors*. Wiley VCH Verlag.

Woods, A. W. 2010 Turbulent plumes in nature. *Annu. Rev. Fluid Mech.* **42**, 391–412.

Zarrebini, M. & Cardoso, S. 2000 Patterns of sedimentation from surface currents generated by turbulent plumes. *AIChE Journal* **46**, 1947–1956.